Newsletters on Stratigraphy, Vol. 49/2 (2016), 383–400 **Article**
Published online February 2016; published in print April 2016

Astronomically tuned age model for the early Eocene carbon isotope events: A new high-resolution $\delta^{13}C_{benthic}$ record of ODP Site 1263 between ~49 and ~54 Ma

V. Lauretano[1], F. J. Hilgen[1], J. C. Zachos[2], and L. J. Lourens[1]

With 8 figures and 4 tables

Abstract. The early Eocene represents a time of major changes in the global carbon cycle and fluctuations in global temperatures on both short- and long-time scales. These perturbations of the ocean-atmosphere system have been linked to orbital forcing and changes in net organic carbon burial, but accurate age models are required to disentangle the various forcing mechanisms and assess causal relationships. Discrepancies between the employed astrochronological and radioisotopic dating techniques prevent the construction of a robust time frame between ~49 and ~54 Ma. Here we present an astronomically tuned age model for this critical time period based on a new high-resolution benthic $\delta^{13}C$ record of ODP Site 1263, SE Atlantic. First, we assess three possible tuning options to the stable long-eccentricity cycle (405-kyr), starting from Eocene Thermal Maximum 2 (ETM2, ~54 Ma). Next we compare our record to the existing bulk carbonate $\delta^{13}C$ record from the equatorial Atlantic (Demerara Rise, ODP Site 1258) to evaluate our three initial age models and compare them with alternative age models previously established for this site. Finally, we refine our preferred age model by expanding our tuning to the 100-kyr eccentricity cycle of the La2010d solution. This solution appears to accurately reflect the long- and short-term eccentricity-related patterns in our benthic $\delta^{13}C$ record of ODP Site 1263 back to at least 52 Ma and possibly to 54 Ma. Our time scale not only aims to provide a new detailed age model for this period, but it may also serve to enhance our understanding of the response of the climate system to orbital forcing during this super greenhouse period as well as trends in its background state.

Key words. Early Eocene hyperthermals, benthic carbon isotopes, astronomical time scale, cyclostratigraphy, Walvis Ridge, Ocean Drilling Program

1. Introduction

The early Eocene was punctuated by multiple global warming events superimposed on the long-term warming trend that started in the late Paleocene and led to the warmest climate conditions of the past 65 Myr during the Early Eocene Climatic Optimum (EECO; e.g., Zachos et al. 2001, 2008, Nicolo et al. 2007, Bijl et al. 2009, Westerhold and Röhl 2009, Stap et al. 2010, Kirtland Turner et al. 2014). On the long-term

Authors' addresses:
[1] Department of Earth Sciences, Faculty of Geosciences, Utrecht University, Heidelberglaan 2, 3584 CS, Utrecht, The Netherlands; E-Mail: v.lauretano@uu.nl, f.j.hilgen@uu.nl, l.j.lourens@uu.nl
[2] Department of Earth and Planetary Sciences, University of California Santa Cruz, 1156 High Street, Santa Cruz, CA 95064, USA; E-Mail: jzachos@ucsc.edu
Corresponding author: E-Mail: v.lauretano@uu.nl

www.borntraeger-cramer.de
DOI: 10.1127/nos/2016/0077 0078-0421/2016/0077 $ 4.50

scale, a significant drop in marine carbonate $\delta^{13}C$ between 58 and 52 Ma has been attributed to a net decrease in organic carbon burial, most likely related to increased fluxes of oxidized CH_4 from the seafloor and of terrestrial organic matter (e.g., Dickens 2003, Komar et al. 2013). On the short-term scale, the series of transient global warming events, known as hyperthermals, caused extreme perturbations of the global carbon cycle and global temperatures superimposed on the long-term warming (e.g., Sluijs et al. 2009, Stap et al. 2010, Zachos et al. 2010, Abels et al. 2012, Kirtland Turner et al. 2014, Littler et al. 2014, Lauretano et al. 2015). The occurrence of these events is marked by dissolution of marine carbonate and negative excursions in carbon and oxygen stable isotopes, and linked to fast injections of isotopically light carbon into the ocean-atmosphere system (Kennett and Stott 1991, Dickens et al. 1995, Lourens et al. 2005, Nicolo et al. 2007, Zachos et al. 2005, 2008, Stap et al. 2010, Littler et al. 2014). The timing of the hyperthermal events suggests that they were paced by orbital forcing (e.g., Cramer et al. 2003, Lourens et al. 2005, Westerhold et al. 2007, 2008, Galeotti et al. 2010, Zachos et al. 2010, Sexton et al. 2011, Kirtland Turner et al. 2014, Littler et al. 2014, Lauretano et al. 2015), specifically by the long- and short-eccentricity cycles.

One of the currently available age models for the early to middle Eocene is based on astronomical tuning of an X-Ray Fluorescence (XRF) Fe-counts record from deep-ocean sediments recovered at ODP Site 1258 (Westerhold and Röhl 2009). The comparison of this Fe-counts record with the bulk carbonate $\delta^{13}C$ isotope record from the same site and splice yields, however, an inconsistent phase relationship between the two proxies in the interval encompassing the EECO, opposite to the coherent patterns observed in the older interval spanning ETM-1 to 3. Other, independent, age models for the early to middle Eocene are based on radioisotopic ages derived from both marine and continental records (Smith et al. 2008, 2014, Aswasereelert et al. 2012, Tsukui and Clyde 2012, Vandenberghe et al. 2012, Machlus et al. 2015). However, around 50 Ma, the comparison between astronomical and radioisotopic age models shows a major discrepancy resulting in a different duration of the magnetochron C23n and a consistent offset of ~0.5 Myr between the two age models up to chron C21r (Vandenberghe et al. 2012). This difference might be a consequence of an overlooked eccentricity cycle in the Fe-counts record, the presence of a hiatus or the poor quality of the magnetostratigraphy at ODP Site 1258 (Vandenberghe et al. 2012). In addition, Westerhold et al. (2015) state that these discrepancies may stem from both uncertainties in the width of chrons in the magnetic anomaly profile of Cande and Kent (1992), as well as in the position and age of the radioisotopic tie points used in GTS2012 (Vandenberghe et al. 2012). Additional high-resolution marine $\delta^{13}C$ records are therefore crucial to provide a precise and consistent temporal framework for this period.

Here we present a high-resolution benthic $\delta^{13}C$ isotope record from ODP Site 1263 (Walvis Ridge), in the east-southern Atlantic, spanning the early Eocene between ~49 and ~54 Ma. Based on this record, we construct an astronomically tuned age model and discuss three different tuning options to the 405-kyr eccentricity cycle. A detailed correlation scheme is then established between our benthic record and the bulk carbonate $\delta^{13}C$ record of ODP Site 1258 (Kirtland Turner et al. 2014). This allows us to test our initial age models, and directly compare our tuning options with alternative age models. Finally, we discuss implications for the polarity time scale and attempt to establish a tuning to the ~100-kyr eccentricity cycle of the La2010d solution (Laskar et al. 2011a), starting from our preferred option, with the aim to investigate the reliability of the newest astronomical solutions.

2. Materials and Methods

2.1 Site location and lithology

Ocean Drilling Program (ODP) Site 1263 (28° 32 S, 2° 47 E, 2717 m present water depth) is located just below the crest of the northeast flank of Walvis Ridge, in the south-eastern Atlantic (Fig. 1) at an estimated paleo-depth of about 1500 m (Zachos et al. 2004). During ODP Leg 208 early Eocene pelagic sections were successfully recovered in four offset holes (A to D), providing a complete sequence of sediments mainly consisting of calcareous nannofossil ooze, chalk and marls. The construction of the composite depth scale from the four holes was based on magnetic susceptibility (MS) and sediment lightness (L*) (Zachos et al. 2004). ODP Site 1263 is ideally suited for this exercise as sedimentation over Walvis Ridge has been relatively uniform over much of the early Paleogene.

Samples were collected at the Bremen Core Repository from Holes A, B and C, according to the shipboard meters composite depth section (mcd) for Site 1263, from ~229 mcd to ~296 mcd. An exception has

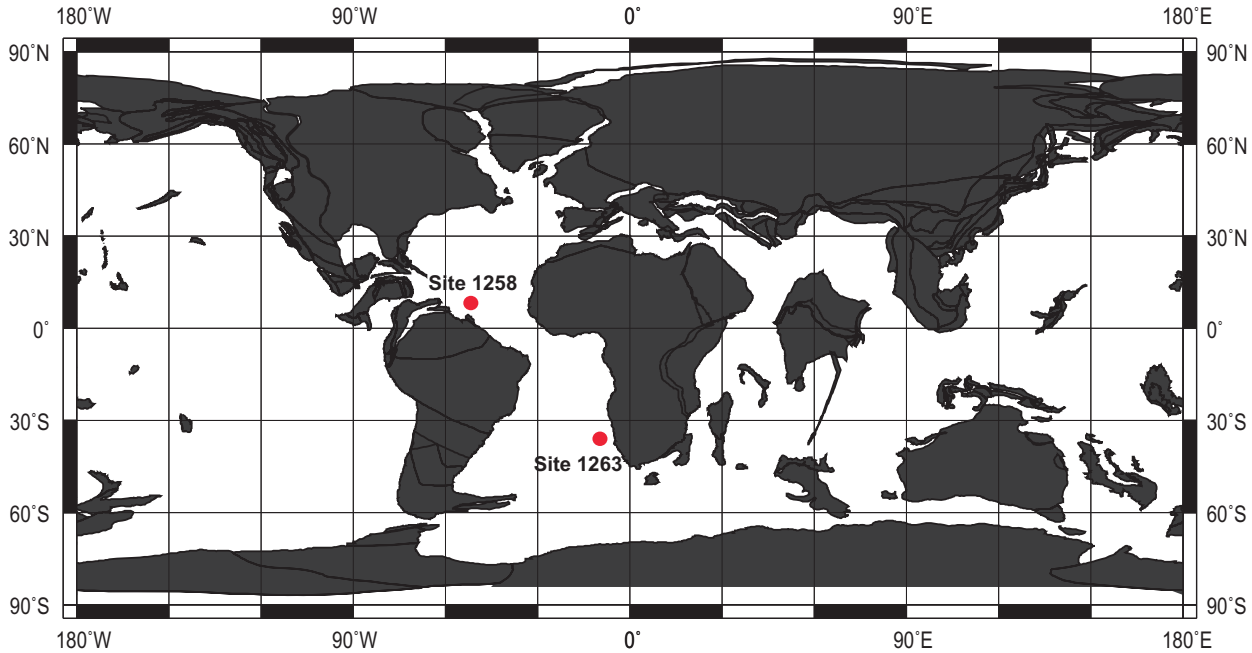

Fig. 1. Paleogeographic reconstruction for the early Eocene (~54 Ma) showing the position of ODP Site 1263 and 1258 (map generated at http://www.odsn.de/odsn/services/paleomap/paleomap.html).

been made for the spliced interval between ~262 and ~268 mcd from which the isotopic results showed an unusual scatter, probably due to contamination of the samples prior to analysis or coring disturbance. For this reason, samples from Hole 1263A core 26H, sections 2–7 were replaced by samples from Hole 1263B core 22H, sections 1–5, partially already included in the revised composite depth scale by Westerhold et al. (2007). This did not require any additional stretching or squeezing of the meter composite depth scale (see Supplementary information).

2.2 Stable isotope analysis

A total of ~1500 samples were used to generate the benthic carbon isotope record, at a 5-cm resolution, including benthic data of Stap et al. (2010) and Lauretano et al. (2015) (Fig. 2 and Appendix A). Multi-specimen samples of shallow infaunal *Nuttalides truempyi* were picked from the > 150 µm fraction and analyzed for stable isotopes by using a KIEL-III automated carbonate preparation device linked online to a Thermo-Finnigan MAT253 mass spectrometer at Utrecht University. All values are reported in standard delta notation relative to VPDB (Vienna Pee Dee Belemnite). Calibrations to the international standard (NBS-19) and to the in-house standard (Naxos) show an analytical precision of 0.03‰ for $\delta^{13}C$.

2.3 Astronomical solution and spectral analysis

Astronomical tuned age models depend on the reliability of the available numerical astronomical solutions for the Solar System (Laskar et al. 2011a, Westerhold et al. 2012). These astronomical solutions however become less reliable further back in time, due to the chaotic behavior of the Solar System. Cyclostratigraphic approaches for the early Paleogene and the Mesozoic therefore rely on the 405-kyr eccentricity cycle, as this is the only cycle to remain stable beyond 50 Ma (Laskar et al. 2004, 2011). First attempts to generate an orbitally tuned time scale for the early Eocene used the La2004 solution (Laskar et al. 2004), and provided a floating time scale based on the tuning to the 405-kyr cycle, anchored to three different options proposed for the age of the PETM (Lourens et al. 2005, Westerhold et al. 2008). At present, the newest orbital solutions (La2010 and La2011) are potentially accurate back to 54 Ma (Laskar et al. 2011a, Westerhold et al. 2012). Tests on the stability of the La2010 (Laskar et al. 2011a) and La2011 (Laskar et al. 2011b) nominal solutions show that only La2010d and La2011 can be applied beyond 47 Ma (Westerhold et al. 2012). The comparison of these solutions to the geological record confirms their stability back to at least 50 Ma, and possibly 54 Ma (Westerhold et al. 2012). Further back in

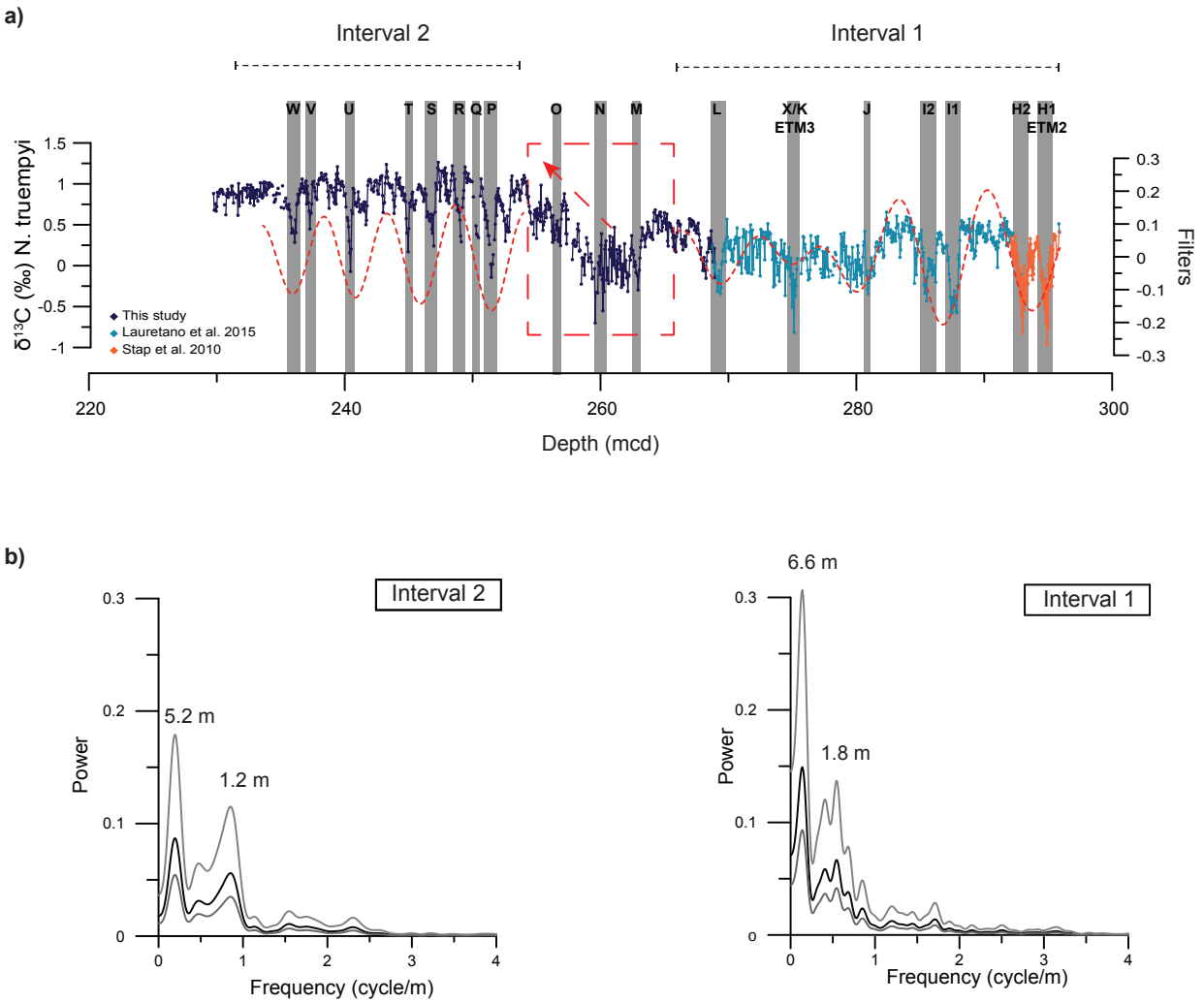

Fig. 2. **a)** Benthic *N. truempyi* $\delta^{13}C$ record from Site 1263 plotted versus depth (mcd). Highlighted intervals represent the position of the early Eocene hyperthermal events and subsequent excursions in the carbon isotope data, labelled alphabetically extending the nomenclature initiated by Cramer et al. (2003). Dashed lines represent bandpass filters applied to the lower and upper intervals. The red box indicates the "problematic interval" characterized by a ~1‰ positive shift in the carbon values. **b)** Power spectra of the two intervals selected for the construction of the age models.

time, only the stable long eccentricity cycle (405-kyr) can reliably be used for tuning. In this study, we initially tuned our carbon isotope record to the 405-kyr eccentricity cycle from the La2010d solution (Laskar et al. 2011a).

For spectral analysis we applied the standard Blackman-Tukey method and Gaussian band pass filtering technique as implemented in the AnalySeries software (Paillard et al 1996).

3. Results

3.1 Benthic $\delta^{13}C$ record of ODP Site 1263

Our benthic $\delta^{13}C$ record reflects a series of negative carbon isotope excursions (CIEs) from ETM2-H2 (Lourens et al. 2005, Stap et al. 2009, 2010) upwards. We identify and label 18 of the excursions with amplitudes ranging between 0.5‰ and 0.8‰, (Fig. 2). In the lower part of our record, these CIEs correspond to the hyperthermal events I1, I2, J, K/X/ETM3 and L (e.g., Cramer et al. 2003, Nicolo et al. 2007, Agnini et al. 2009, Galeotti et al. 2010, Zachos et al. 2010, Slotnick

et al. 2012, Littler et al. 2014, Lauretano et al. 2015). Above this interval, we label 11 additional CIEs in alphabetic order, continuing the nomenclature of Cramer et al. (2003) (Fig. 2 and 5). A pronounced negative peak in the $\delta^{13}C$ at around 260 mcd is preceded by a generally more scattered interval (M-N) that we define as a "problematic" interval for its cyclostratigraphic interpretation (Fig. 2). Above this interval, the average $\delta^{13}C$ background values undergo an increase of ~1‰ between 260 and 253 mcd, while this transition to heavier values is punctuated by shorter negative excursions.

3.2 Astronomical tuning of ODP Site 1263

Cyclostratigraphic interpretation of our $\delta^{13}C$ record of Site 1263 was performed in several steps. First, we separately analyzed the spectral characteristics of two distinct portions of the record: the lower interval between 266 and 296 mcd (Lauretano et al. 2015) and the upper interval between 233 and 253 mcd, since the expression of eccentricity-induced variability is less clear in the problematic interval that marks the shift to heavier $\delta^{13}C$ background values between 253 and 266 mcd (Fig. 2). The interval at the top of our record between 229.78 and 233.60 mcd was not included in this analysis because of strong coring disturbance identified in this part (Westerhold et al. 2015). The lower interval revealed spectral peaks at periods of 6.6 and 1.88 m, which were interpreted by Lauretano et al. (2015) to reflect the 405- and 100-kyr eccentricity cycles, in agreement with the long-term variability previously found in MS, a* and Fe-counts records of Site 1263 (Lourens et al. 2005, Westerhold et al. 2007). The upper interval revealed similar strong peaks, though with slightly reduced wavelength at 5.2 m and 1.2 m, which we similarly interpreted as reflecting the expression of the 405- and 100-kyr eccentricity cycles.

We applied a Gaussian filter centered at a frequency of 0.15 ± 0.045 cycles per meter for the lower interval, and tuned the filtered component to the extracted 405-kyr eccentricity cycle of the La2010d solution (Fig. 3; see also Lauretano et al. 2015). Our tuning approach is based on the same phase relation as in previous studies, i.e. minima in $\delta^{13}C$ correspond with maxima in the 405-kyr eccentricity cycle and vice versa (Lourens et al. 2005, Westerhold et al. 2007, Zachos et al. 2010). We anchored our tuning by correlating the minimum in the $\delta^{13}C$-filtered component corresponding to ETM2-H2 (Stap et al. 2010) to the maximum in the 405-kyr cycle around 54 Ma (Fig. 3d). As starting point, we assigned an age of 54.09 ± 0.02 Ma to ETM2, according to option 2 of Westerhold et al. (2008). The lower interval was therefore tuned to 5 successive maxima in the 405-kyr eccentricity cycle between ~54 and 52.4 Ma. We used this interval as the fixed backbone of our age model to construct and test three different age model options for the younger part of our record (Table 1).

The ~5.2-m cycle was extracted from the $\delta^{13}C$ record of the upper interval, using a band pass filter centered at a frequency of 0.19 ± 0.06 cycles/m, reflecting the presence of four 405-kyr eccentricity -related cycles (Fig. 2). To establish our tuning options we considered that 1, 2 or 3 405-kyr eccentricity-related cycles are present in the problematic interval (Fig. 3a–c). According to these three age models the age for the top of our record arrives at 49.85, 49.45 or 49.05 Ma, respectively. Accordingly, our record comprises 11, 12 or 13 405-kyr cycles, which in turn correspond to a total of 15, 16, or 17 405-kyr cycles for the early Eocene between the PETM and the top of our record (Westerhold et al. 2007).

The consequences for the calculated average sedimentation rates for each of the three age models are presented in Figure 4a. The 1-cycle model would imply an almost doubling in sedimentation rate across the problematic interval while the 2-cycle age model results in smooth changes in sedimentation rate and represents the most conservative solution with an on average constant sedimentation rate throughout the study interval of 1.4 cm/kyr. The 3-cycle age model translates into a decrease in sedimentation rate across the problematic interval. The 2-cycle age model provides the best fit of the inferred cycle pattern with 405-kyr eccentricity, but an opposite phase relation is observed around 51.7 Ma coincident with the $\delta^{13}C$ minimum in the problematic interval between cycles 10 and 11 (Fig. 3b). This discrepancy can be explained by minor changes in sedimentation rate in combination with the correspondence of this interval with a ~2.4 Myr eccentricity minimum (see Paragraph 4.2). The 3-cycle age model reveals an apparent misfit with 405-kyr eccentricity between 51.2 and 51.8 Ma, but it results in a more realistic detection of the 100-kyr cycle and a better fit of the $\delta^{13}C$ minimum (i.e., $Ec_{405}11$) in the problematic interval (Fig. 3c).

3.3 Comparison with ODP Site 1258

To further test our three 405-kyr eccentricity based age models, we compared the $\delta^{13}C$ of ODP Site 1263 with the bulk carbonate $\delta^{13}C$ record of ODP Site 1258

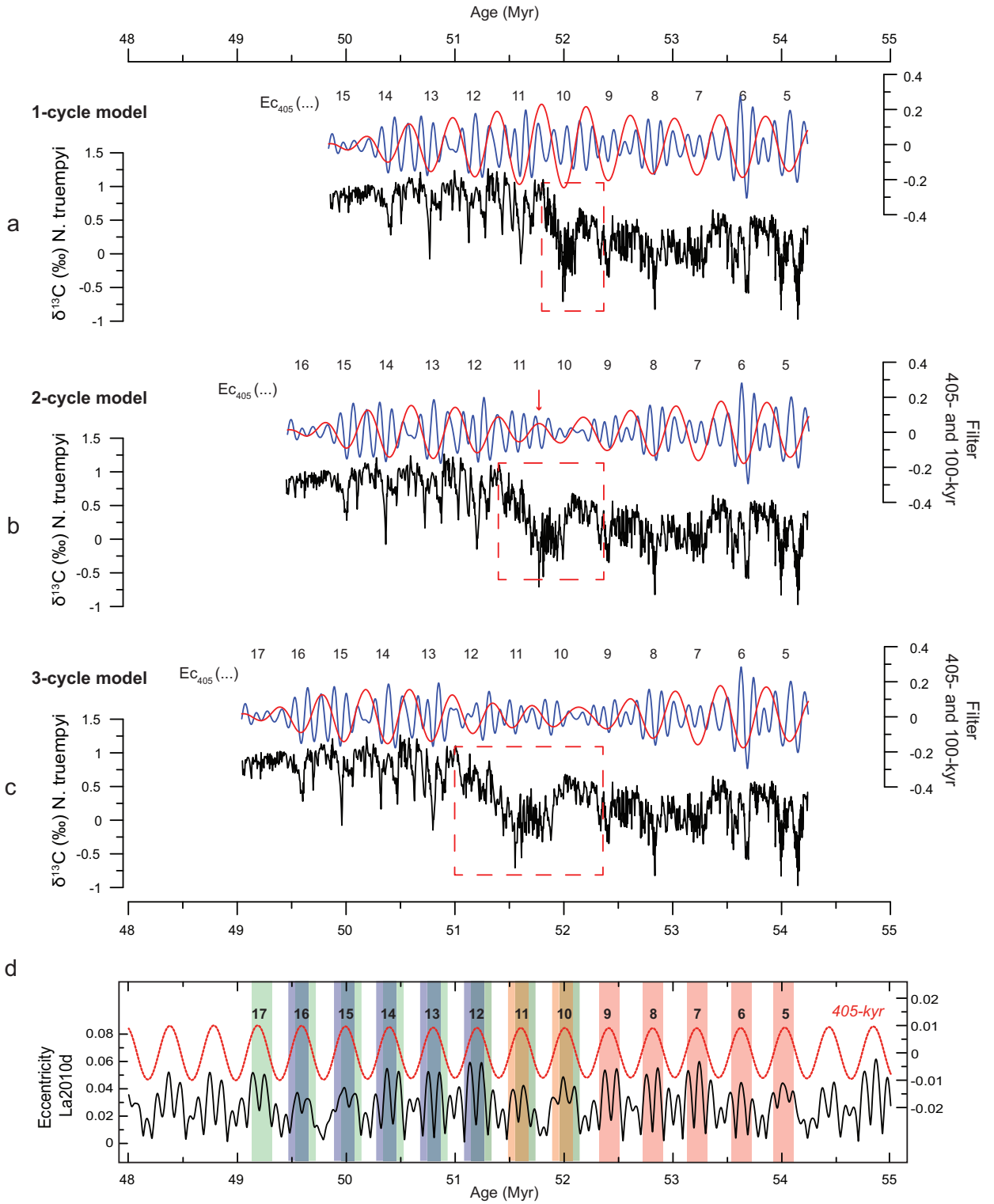

Fig. 3. **(a, b, c)** Astronomically tuned age model options for the benthic $\delta^{13}C$ record of Site 1263 and related 100- and 405-kyr band pass filters (Filter details: 0.0085 ± 0.0025 and 0.002469 ± 0.0005, respectively). The three options refer to the number of 405-kyr cycles contained in the "problematic" interval to heavier $\delta^{13}C$ values. **d)** The age model options are based on the tuning to the 405-kyr component of the La2010d (Laskar et al. 2011a). Eccentricity related cycles are numbered following Westerhold and Röhl (2009), starting from the PETM.

Table 1 Age-depth tie points of the three age model options based on the tuning to the long-eccentricity cycle extracted from the orbital solution La2010d (Laskar et al. 2011a).

Depth (mcd)	1-cycle model (kyr)	2-cycle model (kyr)	3-cycle model (kyr)
233.62	50192.5	49789.5	49386.5
235.92	50394.0	49991.0	49588.0
238.42	50595.0	50192.5	49789.5
240.81	50796.5	50394.0	49991.0
243.31	50998.0	50595.0	50192.5
245.91	51199.0	50796.5	50394.0
248.66	51400.5	50998.0	50595.0
251.45	51602.0	51199.0	50796.5
253.95	51804.0	51400.5	50998.0
266.25	52207.5	52207.5	52207.5
269.35	52409.5	52409.5	52409.5
272.35	52611.5	52611.5	52611.5
274.89	52813.5	52813.5	52813.5
277.09	53015.5	53015.5	53015.5
279.94	53217.5	53217.5	53217.5
283.24	53419.5	53419.5	53419.5
286.64	53622.0	53622.0	53622.0
290.13	53824.0	53824.0	53824.0
293.63	54027.0	54027.0	54027.0
295.78	54230.0	54230.0	54230.0

(Kirtland Turner et al. 2014), based on the astronomically tuned age model of Westerhold and Röhl (2009). ODP Site 1258 is located on Demerara Rise in the equatorial western Atlantic at a present-day water depth of ~3200 m and estimated paleodepth of ~3000 m during the Eocene (Sexton et al. 2006). The bulk carbonate record is dominated by calcareous nannofossils (Sexton et al. 2006) and thus expected to mainly reflect surface water signals, while our benthic record reflects deep-water conditions. Although the bulk and benthic $\delta^{13}C$ records carry the expression of different ecological conditions, they often co-vary indicating that they both portray (isotopic) changes in the global carbon cycle (e.g., Grant and Dickens 2002, Reghellin et al. 2015). In particular this is confirmed by the close resemblance between the bulk carbonate and benthic $\delta^{13}C$ records at ODP Sites 1258, 1263 and 1262 (Stap et al. 2010, Littler et al. 2014, Kirtland Turner et al. 2014) and the similarities between these records. Changes in the carbon cycle on eccentricity time scales can be explained by changes in the burial ratio of carbonate to organic carbon due to weathering (Cramer et al. 2003, Ma et al. 2011). During phases of eccentricity maxima, increased weathering and nutrient supply could drive minima in $\delta^{13}C$ by increasing the carbonate to organic carbon burial ratio (Cramer et al. 2003, Ma et al. 2011, Westerhold et al. 2015). These weathering-induced changes appear to affect the whole water column (Ma et al. 2011), thus explaining the consistent coupling between surface and deep-water signals expressed by the trends in the $\delta^{13}C$ records.

Based on similarity between the records, we aligned both $\delta^{13}C$ records in the depth domain, using 30 characteristic features as tie points (Fig. 5 and Table 2). We correlated the pronounced CIEs found at Site 1263 to the CIEs identified at Site 1258 and labelled them with reference to the magnetostratigraphic information available for this site (Kirtland Turner et al. 2014) (Fig. 5). At Site 1258, these excursions have been interpreted and labelled as potential hyperthermal events; in lack of additional data to support this claim, we simply extended the alphabetical nomenclature introduced by Cramer et al. (2003) to describe the transient events in the carbon record.

Subsequently, we transferred our three age models from Site 1263 to Site 1258, and compared the resulting age-depth relationships of Site 1258 with that of Westerhold and Röhl (2009) in Figure 4b. For this comparison, we refrained from using the depth-correlation lines in the problematic interval of Sites 1263/1258 (253–266 mcd/71–86 rmcd) as age tie points (shown in Fig. 5) to increase the degree of freedom that

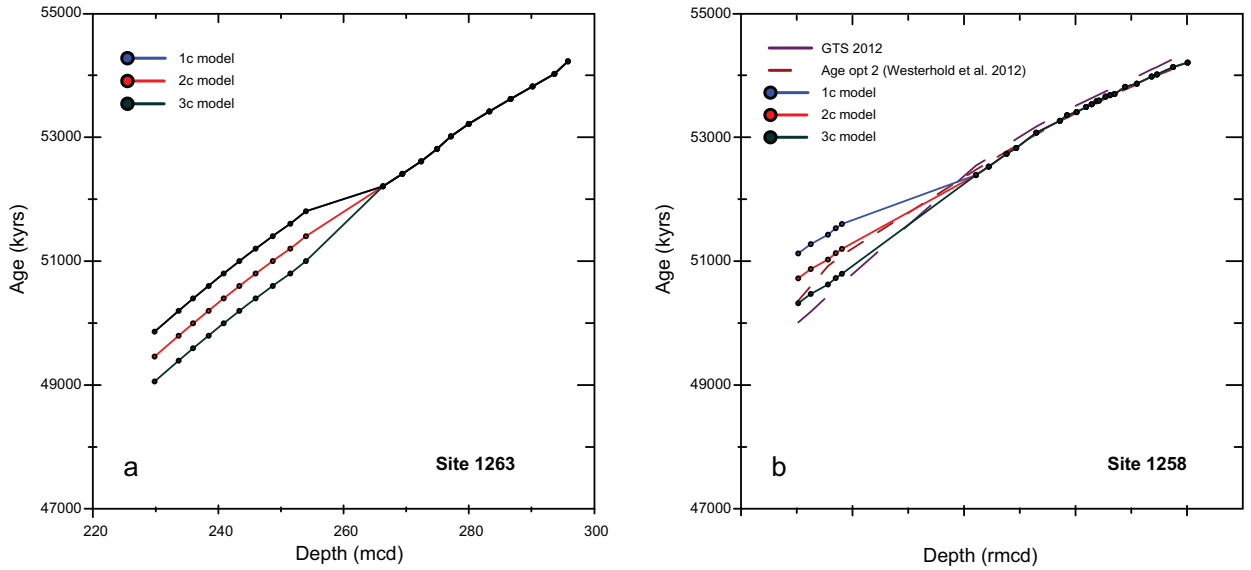

Fig. 4. **a)** Age vs depth plot of the three age model options of Site 1263. **b)** Age vs depth plot of the three age model options established for Site 1263, the initial age model by Westerhold and Röhl (2009) and ages from the Geological Time Scale 2012 (GTS2012) (Vandenberghe et al. 2012).

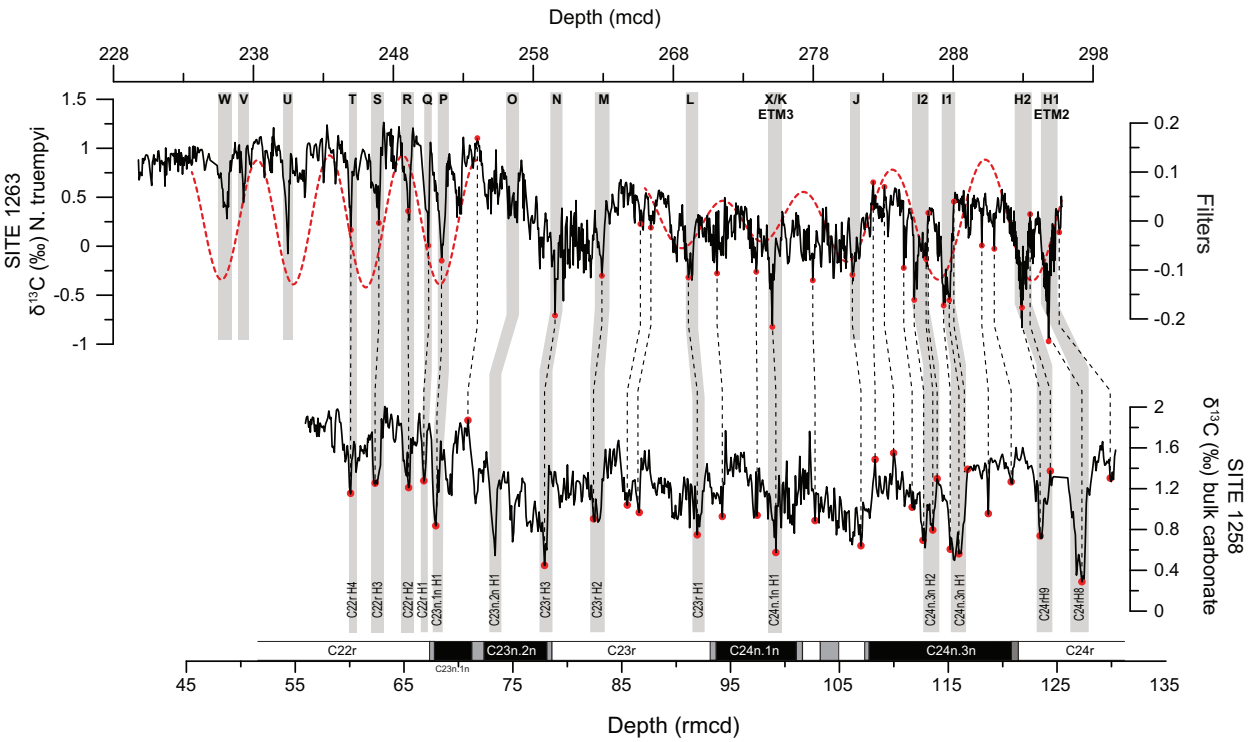

Fig. 5. Correlation scheme between the benthic $\delta^{13}C$ record of Site 1263 and the bulk carbonate $\delta^{13}C$ record of Site 1258 (Kirtland Turner et al. 2014). Red dots correspond to the depth tie points selected between the records based on recognizable features between the two records. Grey bars indicate the position of the negative carbon excursions with relative labels by Kirtland Turner et al. (2014) for Site 1258.

could reveal possible uncertainties in the age models through this interval.

Similarly as for Site 1263, the 1- and 3-cycle options for Site 1258 result in a distinct change in sedimentation rates around 52 Ma (Fig. 4b). Clearly our 2-cycle age model largely fits the initial tuning (option 2) by Westerhold and Röhl (2009), though both age models start to diverge significantly above 70–80 rmcd (Fig. 4b). In Figure 6, our benthic $\delta^{13}C$ record of Site 1263 and the bulk carbonate $\delta^{13}C$ record from Site 1258 are compared against time, using our 2-cycle option and the initial age model by Westerhold and Röhl (2009). Both records correlate unambiguously in the lower interval (rmcd 90–130) corresponding to the 405-kyr eccentricity related cycles labelled $Ec_{405}5$ to $Ec_{405}9$ by Westerhold & Röhl (2009). Consistent patterns are identified in both $\delta^{13}C$ records between ETM2 and ETM3, allowing for a univocal cyclostratigraphic interpretation on the 405-kyr scale in this interval (see also Lauretano et al. 2015).

The 405-kyr cycle patterns and underlying $\delta^{13}C$ records covering cycles $Ec_{405}10$ to $Ec_{405}11$ show good agreement between both sites, with the exception of the more distinct short-term negative isotope excursions found at Site 1258 during $Ec_{405}11$, i.e. during the long-term shift in the carbon isotope record (Fig. 6a–c). These excursions, although present, are far less pronounced at Site 1263, probably indicating condensed intervals due to dissolution (or lower sedimentation rates) or small gaps in our record. Nevertheless, the pattern found at Site 1258 suggests that only 2×405-kyr eccentricity cycles are present within this

Table 2 Depth tie points between ODP Sites 1263 and 1258 and their relative ages according to the three age models.

Site 1263 (mcd)	Site 1258 (rmcd)	1-cycle model (kyr)	2-cycle model (kyr)	3-cycle model (kyr)
244.96	60.28	51125.6	50723.0	50320.5
246.96	62.53	51276.2	50873.7	50471.0
249.10	65.61	51428.9	51026.4	50623.4
250.45	67.01	51533.4	51130.6	50727.9
251.45	68.11	51601.8	51198.8	50796.3
254.00	71.06			
256.50	73.56			
260.15	78.10			
262.90	82.60			
265.65	85.70			
266.40	86.80			
269.08	92.13	52392.0	52392.0	52392.0
271.13	94.43	52529.6	52529.6	52529.6
273.93	97.63	52737.1	52737.1	52737.1
275.08	99.35	52830.6	52830.6	52830.6
277.97	102.95	53077.7	53077.7	53077.7
280.80	107.17	53270.1	53270.1	53270.1
282.29	108.47	53361.4	53361.4	53361.4
283.09	110.17	53410.4	53410.4	53410.4
284.47	111.87	53492.9	53492.9	53492.9
285.22	112.87	53537.6	53537.6	53537.6
286.07	113.77	53588.3	53588.3	53588.3
286.22	114.17	53597.2	53597.2	53597.2
287.32	115.37	53661.5	53661.5	53661.5
287.72	116.17	53684.6	53684.6	53684.6
288.05	116.97	53703.7	53703.7	53703.7
290.05	118.87	53819.2	53819.2	53819.2
290.94	120.97	53870.8	53870.8	53870.8
292.92	123.63	53985.7	53985.7	53985.7
293.5	124.57	54019.4	54019.4	54019.4
294.82	127.47	54139.3	54139.3	54139.3
295.58	130.07	54211.1	54211.1	54211.1

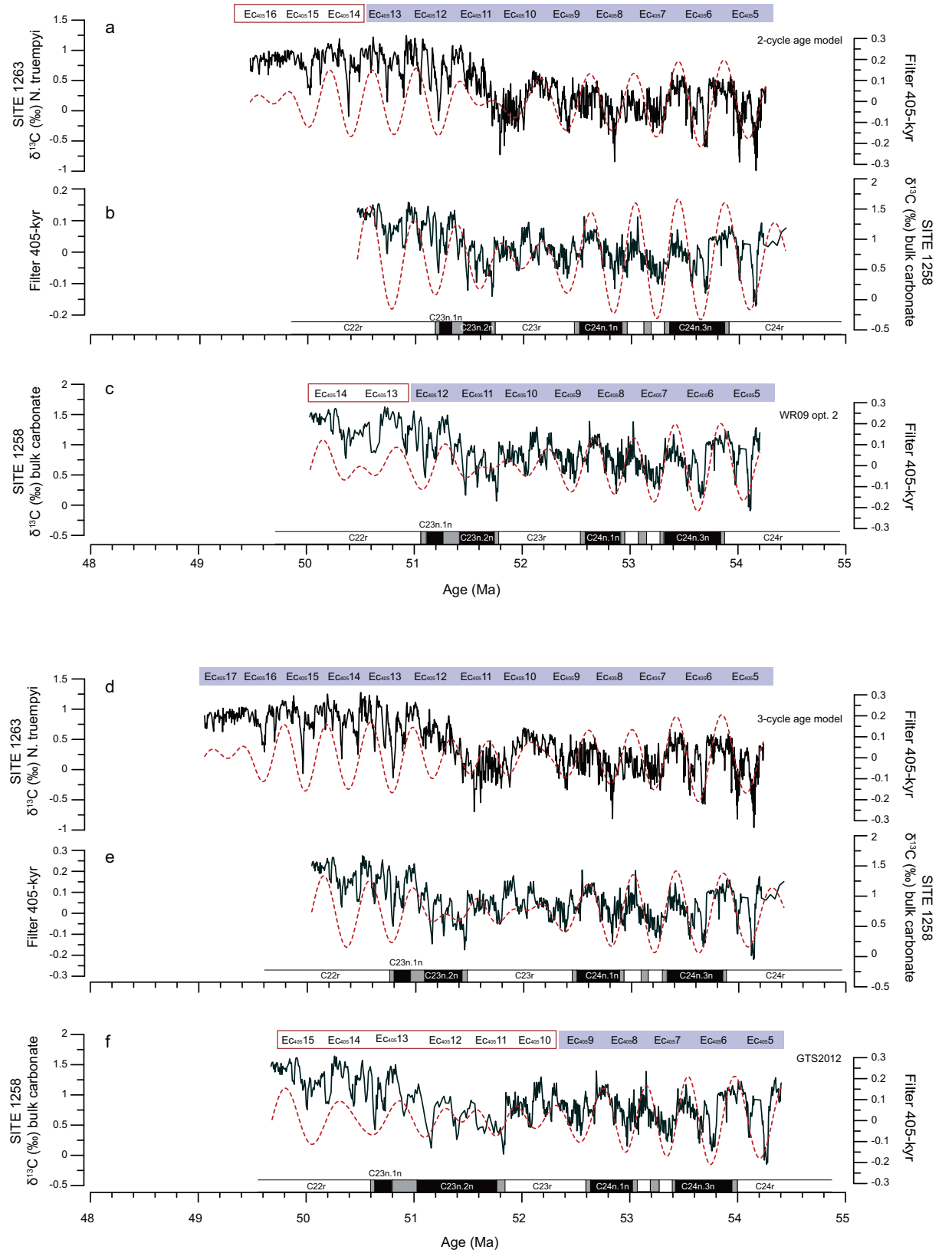

Fig. 6. **(a–c)** Comparison between our 2-cycle age model option for Site 1263 and 1258 and the initial age model by Westerhold and Röhl (2009). **(d–e)** Comparison between our 3-cycle age model option for ODP sites 1263 and 1258 and ages from Geological Time Scale 2012 (GTS2012, Vandenberghe et al. 2012).

problematic interval, as found by Westerhold and Röhl (2009).

The 2-cycle option also yields a good correlation between Sites 1263 and 1258 from $Ec_{405}12$ to the top of the bulk $\delta^{13}C$ record, although significantly off from the initial age model by Westerhold and Röhl (2009). In comparison to our results of Site 1263, Westerhold and Röhl (2009) seem to have stretched this interval considerably to accommodate an additional 405-kyr cycle in this part of 1258 (Fig. 6c). Assuming that our correlation scheme between both sites is robust, we consider the occurrence of this additional cycle less likely, since it would result in a proportional stretching of the $\delta^{13}C$ record from Site 1263 for which we do not have evidence.

An alternative age model for Site 1258 was presented in the Geologic Time Scale 2012 (GTS2012), which reviews the astronomical tuning of Westerhold and Röhl (2009), but includes additional radioisotopic dates and sea floor spreading rates (Vandenberghe et al. 2012). For comparison, we have included the GTS2012 age model in the age-depth plot of Site 1258 (Fig. 3b), using the magnetostratigraphy of ODP Site 1258 and applying the GTS2012 chron boundary ages as constraints (see also Kirtland Turner et al. 2014, Supplementary information). Evidently, the GTS2012 ages are in much better agreement with our 3-cycle age model, but with clear differences in age. In particular, the lower (upper) part of the record is significantly older (younger) according to Vandenberghe et al. (2012)

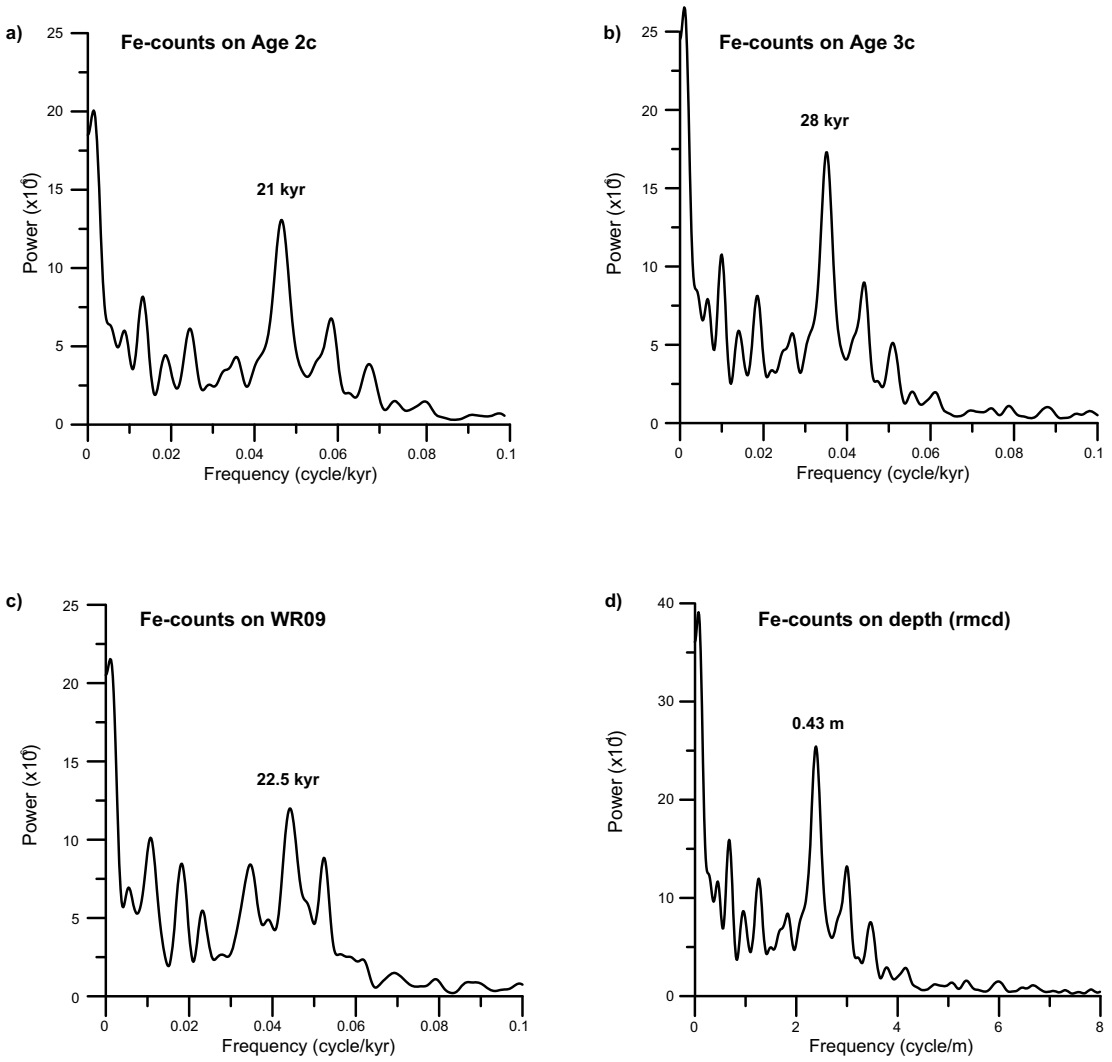

Fig. 7. Power spectra of the Fe-record in the problematic interval from of Site 1258 using a) 2-cycle age model: b) 3- cycle age model and c) the initial age model by Westerhold and Röhl (2009) d) depth scale (rmcd).

than compared to our tuning (Fig. 3b). Since our 1-cycle option is distinctly off from all the other age models presented, it will be discarded from further evaluation.

A comparison between the extracted filtered 405-kyr components of the $\delta^{13}C$ records from Sites 1263 and 1258 plotted on our 3-cycle age model and the GTS2012-based age model is shown in Figure 6 (d–f). Clearly, GTS2012 assigns older ages to the eccentricity related cycles $Ec_{405}5$ to $Ec_{405}9$ than we propose. In addition, the 405-kyr filtered component and the $\delta^{13}C$ record start to reveal major discrepancies from $Ec_{405}10$ onwards in GTS2012 when the amplitude of the filtered signal becomes strongly reduced. In particular, the interval corresponding to cycles $Ec_{405}11$–$Ec_{405}12$ becomes significantly stretched in GTS2012, which implies an almost doubling of the time span in between the two major negative excursions (N–O) at the onset of the shift in the carbon isotope records. Therefore the GTS2012 age model arrives at a much younger age for the top part of the record to accommodate nearly one extra 405-kyr cycle compared to our 3-cycle age model and that of Westerhold and Röhl (2009), and two extra cycles compared to our 2-cycle age model. Moreover, the filtered 405-kyr components of GTS2012 and our 3-cycle age model are anti-correlated for $Ec_{405}12$ to $Ec_{405}14$ (Fig. 5).

To further evaluate our 2- and 3-cycle age models, we analyzed the spectral characteristics of the XRF-based Fe records (Westerhold and Röhl 2009) from the problematic interval between 70 and 91 rmcd at Site 1258 (Fig. 7d). The spectra reveal strong peaks corresponding to periods of 21- and 28-kyr according to the 2 and 3-cycle age model, respectively (Fig. 7a–b). The 21-kyr period is close to the 22.5-kyr cycle detected on the basis of the initial age model of Westerhold and Röhl (2009), who interpreted this cycle as the imprint of precession (Fig. 7c). Clearly, the 28-kyr period in the Fe spectrum according to our 3-cycle age model does not correspond to the theoretical values for precession during this time interval and is also too far off to be explained by obliquity forcing. The inclusion of the extra 405-kyr cycle compared to the 2-cycle age model causes the shift of the precession-related peak from ~21- to 28-kyr, invalidating the robustness of the 3-cycle model. Therefore we consider the 2-cycle age model as the best possible age model for the problematic interval. This is corroborated by the relative constant sedimentation rates for both Site 1263 and 1258 (Fig. 4).

4. Discussion

4.1 Implications for the Global Polarity Time Scale

One of the main problems in constructing the GTS2012 was the significant discrepancy observed between the astronomical age model (i.e., option 2 of Westerhold and Röhl 2009) and the radioisotopic age model around 50 Ma (Vandenberghe et al. 2012). Specifically, the astronomical age model resulted in a much shorter duration of C23n.2n, as compared to – for instance – C23r than radioisotopic age models, leading to a consistent offset of ~0.5 Myr with astronomical ages of reversal boundaries being abruptly older from C23n up to C21n (Vandenberghe et al. 2012). The resultant 2:1 ratio in duration between C23r and C23n.2n was in particular inconsistent with the approximately 1:1 width ratio observed in seafloor anomaly profiles from different ocean basins (Cande and Kent 1995) used as reference in GTS2012. Possible explanations for the observed discrepancy lie in the quality of the magnetostratigraphy, a hiatus or an overlooked 405-kyr cycle in Site 1258 proxy records on which the astronomical age model was based for this time period (Vandenberghe et al. 2012), but may also stem from uncertainties in the width of the magnetic anomaly profile of Cande and Kent (1992), errors in absolute ages for the calibration tie points, and position of magnetic reversals (Westerhold et al. 2015).

The convincing correlation between the $\delta^{13}C$ records of Sites 1263 and 1258 indicates that the presence of a significant hiatus in Site 1258 is unlikely, as this would imply that such a hiatus would cover exactly the same interval at both these sites located on opposite sides of the Atlantic Ocean. In addition, the spectrum of the Fe-counts record using our preferred 2-cycle age model reveals a clear precession signal, as similarly documented by Westerhold and Röhl (2009), corroborating the robustness of the astronomical tuning approach within the interval of C23r. The discrepancies between GTS2012 and the astronomically tuned age models thus remain unsolved and therefore question the reliability of the radioisotopic ages, the magnetostratigraphic constraints of Site 1258 and/or the robustness of the South Atlantic anomaly profile. Moreover, the quality of the selected age tie points in the radioisotopic age model of Vandenberghe et al. (2012) did not meet strict requirements – single crystal Ar/Ar sanidine or U/Pb zircon ages unambiguously tied to chron boundaries via reliable magnetostratigraphy –

due to the scarcity of such tie points in this interval. This may have added to the uncertainty in the final age model proposed by Vandenberghe et al. (2012).

On the other hand, the original magnetostratigraphy of Site 1258 (Suganuma and Ogg 2006) was substantially revised and improved by Westerhold and Röhl (2009). As discussed in Westerhold and Röhl (2009), Suganuma and Ogg (2006) suggested that the uppermost part of C23n in Hole 1258B and/or the overlying Chron 22r in Hole 1258A was most likely truncated by an unrecognized fault, which could explain the offset in the planktonic foraminifer Zone E6/E5 (Berggren and Pearson 2005, Wade et al. 2011) (Zone P8/P7 sensu Berggren et al. 1995). Westerhold and Röhl (2009) tackled this problem by presenting new nannofossils data, i.e. the HO of *T. orthostylus* which was found by Agnini et al. (2006) close to the base of C22r in the Possagno section (Italy). However, according to Westerhold and Röhl (2009), this event occurs within C23n and therefore does not provide a very reliable age constraint either. The upper constraint of C23n in Site 1258 remains therefore debatable.

Finally, it appears that the spreading rates based on CK95 (Cande and Kent 1995) are smaller in C23n.2n than in C23r within three different oceanic basins (Bouligand et al. 2006). This consistency indicates that the duration ratio of C23n.2n vs. C23r should be smaller (i.e., C23n.2n should be shorter and/or C23r should be longer), which may point to a fundamental problem in the critical interval of the South Atlantic anomaly profile, used by Cande and Kent (1995) and by Vandenberghe et al. (2012).

4.2 Towards a 100-kyr eccentricity tuned age model

Based on our results, we consider the 2-cycle age model as the most plausible age model since it results in steadiness of sedimentation rate across the problematic middle interval for both Site 1263 and 1258. Starting from this age model, we attempted to establish a tuning to 100-kyr eccentricity. Although such a fine tuning is considered risky in this time period due to uncertainties in the stability of the orbital solution beyond 50 Ma (Laskar et al. 2011a, Westerhold et al. 2012, 2015), we base our approach on the tight match between the geological record and the orbital solution, which highlights the good fit between variations in our proxy record and

Table 3 Ages of the chron boundaries according to different age models. **CK95:** Cande & Kent (1995); **GTS2012:** Geological Time Scale 2012 (Vandenberghe et al. 2012); **WR09:** Westerhold and Röhl (2009); **S2014:** Smith et al. (2014); **TC2012:** Tsukui and Clyde (2012).

	CK95		GTS2012						WR 09		S2014		TC2012 new WW		this paper 2 cycle		this paper 3 cycle	
			astro		radio		combined											
C21n	1642		1895		1620		1620						2460					
C21r	1131		1265		1220		1220		1265				1118					
C22n	677		638		780		780		638		290		900					
C22r	1064		1469		1280		1280		1469		340		920					
C23n.1n	168		224		210		210		224				160		159		208	
C23n.1r	101	*965*	72	*675*	130	*1210*	130	*1210*	72	*675*	1640	*1640*	100	*930*	55	*509*	73	*676*
C23n.2n	696		379		870		870		379				670		295		395	
C23r	621		800		790		790		800		1170		570		781		1016	
C24n.1n	299		390		380		450		390				270		458		458	
C24n.1r	94		125		120		130		125				110		162		162	
C24n.2n	44	*983*	75	*1299*	60	*1250*	80	*1370*	75	*1299*			50	*1040*	67	*1390*	67	*1390*
C24n.2r	102		142		130		140		142				110		142		142	
C24n.3n	444		567		560		570		567				500		561		561	

Table 4 Age tie points based on the benthic $\delta^{13}C$ record from Site 1263 and used in the final tuning to the La2010d eccentricity cycle, starting from the 2-cycle age model.

Site 1263 CIEs (This study)	Site 1258 (Kirtland Turner et al. 2014)	Ages after tuning to La2010d eccentricity
W		49984.47
V		50077.16
U		50382.83
T	C22rH4	50745.35
S	C22rH3	50873.68
R	C22rH2	51044.12
Q	C22rH1	51138.00
P	C23n.1nH1	51238.98
O	C23n.2nH1	51347.19
N	C23rH3	51611.14
M	C23r H2	51884.25
L	C23r H1	52089.57
K/X/ETM3	C24n.1nH1	52484.60
J		52860.31
I2	C24n.3nH2	53229.85
I1	C24n.3nH1	53531.47
H2	C24rH9	53627.40
(Elmo/H1/ETM2)	C24rH8	53916.31

the patterns of the orbital solution. For this purpose we primarily used the characteristic patterns, i.e. CIEs, of the $\delta^{13}C$ records in combination with the results of 100-kyr band pass filtering rather than the filters alone, as these are very sensitive to changes in bandwidth and/or sedimentation rate (Table 4).

Starting from our tuning to the long eccentricity cycle, the tuning to the 100-kyr eccentricity is relatively straightforward for the interval between 49.5 and 50.8 Ma, where we correlated the double 100-kyr peaks of $Ec_{405}13$ to 15 (S to W) in $\delta^{13}C$ to pronounced maxima in the eccentricity curve resembling this pattern. Next, the four well-developed negative carbon peaks (P–R) of $Ec_{405}12$ are in excellent agreement with the four distinct 100-kyr maxima around ~51.2 Ma (Fig. 8). The more negative values in the problematic interval (N–M) at ~52 Ma fit with the interval of the reduced amplitude of the 100-kyr eccentricity cycle in $Ec_{405}10$, which results from a minimum in the very long eccentricity cycle (~2.4 Myr), in agreement with observations for Site 1258 (Westerhold and Röhl 2009). In this respect, we suggest that the pronounced negative isotope excursion at 260 mcd in Site 1263 merely corresponds to the expression of the youngest 100-kyr eccentricity-related cycle of $Ec_{405}11$ rather than an anti-phase relationship with the 405-kyr eccentricity cycle as indicated by our 2-cycle option.

The tuning of the lower interval is easily resolved between L and I2. However, the position of ETM2 is questionable, as Westerhold et al. (2007) linked this event to the first (oldest) 100-kyr eccentricity maximum in the 405-kyr maximum, while Lourens et al. (2005) tuned it to the second, most pronounced 100-kyr eccentricity maximum. Uncertainties in the solution in this time period prevent a final tuning of ETM2 on the short-eccentricity scale. However, tuning the first of the "paired events" to the second, most pronounced eccentricity maximum is consistent with the number of 100-kyr eccentricity related cycles between ETM2-H2 and I1–I2, and the pattern and tuning of I1–I2. We therefore adopt this option for our tuning of this interval (Fig. 8), until improved orbital solutions become available.

Based on our observations, the patterns of short-eccentricity in the La2010d solution are in good agreement with the variations in the $\delta^{13}C$ records of Sites 1263 and 1258, suggesting that the solution might be reliable to at least 52 Ma and possibly even 54 Ma. This conclusion is in line with Laskar et al. (2011a), stating that the La2010 solution is reliable over more than 50 million years, and with Westerhold et al. (2012), who also argued that the La2011 solution is reliable back to ~54 Ma. More recently, Westerhold et al. (2015) found inconsistencies in a comparison of proxy records of various ODP sites over the middle Eocene suggesting a possible issue with the newest La2011 solution.

The resulting age model applied to both records translates in an on average constant sedimentation rate of 1.5 cm/kyr and 2 cm/kyr for Site 1263 and 1258, respectively, with a minor decrease from ~51.8 Ma, coincident with the transition to heavier carbon values. Spectral power is concentrated at short- and long-eccentricity frequencies, which is not surprising in view of the tuning method.

Our tuning approach is based on the phase relationship between the early Eocene CIEs events and eccentricity maxima, as initially proposed by Lourens et al. (2005), and the tight match between the geological record and the astronomical solution appears to support this phase relationship. However, Smith et al. (2014) recently linked the occurrence of the CIEs related to hyperthermals to 405-kyr eccentricity minima, based on studies of the continental Green River Formation from which numerous age models have been developed over the last decade (Machlus et al. 2008,

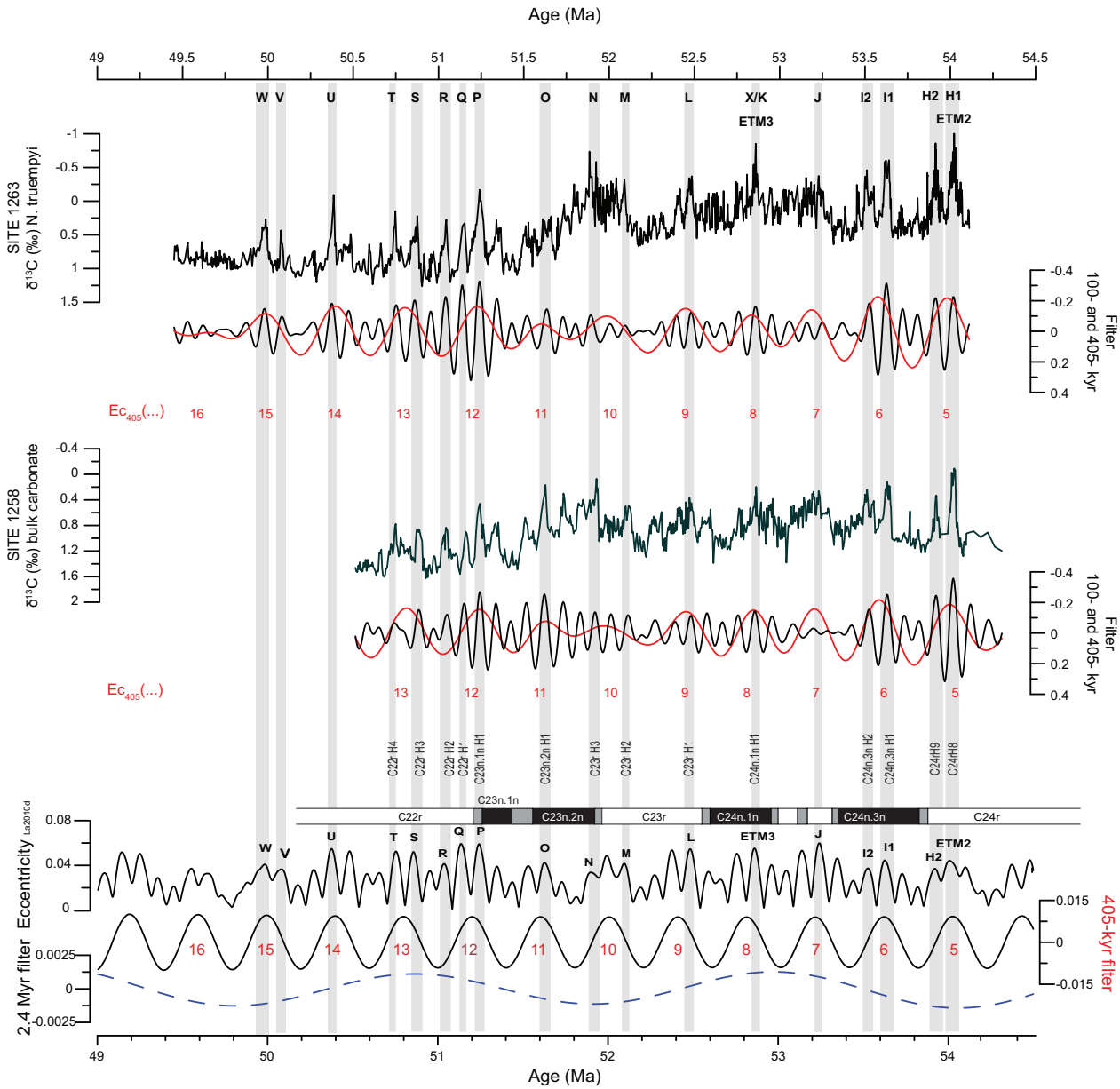

Fig. 8. Final tuning to the short-eccentricity in La2010d starting from the 2-cycle age model for Site 1263. Interpolated ages were transferred to Site 1258 by using the correlation tie points previously selected.

2015, Smith et al. 2008, 2014, Aswasereelert et al. 2012, Tsukui and Clyde 2012). Green River and marine-based age models can in principle be compared using magnetostratigraphic correlations and ages of chron boundaries. However, such a comparison is complicated by ongoing uncertainties in the ages of ash layers in the Green River Fm. Recent U-Pb ages of ash layers are up to 250 kyr younger than previously obtained Ar-Ar ages (Machlus et al. 2015), and the magnetostratigraphy and its correlation to the GPTS result in anomalously long or short (sub)chrons (i.e. the short C22r in the tiered age model of Smith et al. 2014) as compared to Cande and Kent (1995) and Vandenberghe et al. (2012). These limitations are likely responsible also for the opposite phase relation between hyperthermals and eccentricity inferred by Smith et al. (2014), with hyperthermals corresponding to minima. In view of these uncertainties and discrepancies between current Green River age models, we here refrained from making detailed comparisons with

our marine-based astronomical age model (ages and durations are reported in Table 3). A more detailed discussion on this specific issue and the comparison between marine and terrestrial records can be found in Westerhold et al. (2015).

5. Conclusions

Our high-resolution benthic $\delta^{13}C$ record from ODP Site 1263 offers the opportunity to provide a robust temporal framework for long- and short-term variability in the carbon cycle during the early Eocene (~49–54 Ma). We evaluated three tuning options for an astronomical age model, differing in the number of eccentricity-related cycles (405-kyr) in the so-called "problematic" interval, during which average $\delta^{13}C$ values undergo a positive shift of ~1‰. While the presence of only one cycle in this interval can be excluded, it is more difficult to discriminate between the 2- and 3-cycle options. The correlation to the bulk carbonate $\delta^{13}C$ record from Site 1258 (Kirtland Turner et al. 2014) allowed to further test our age models and to compare them with the initial astronomical age model of Westerhold and Röhl (2009). Our 2-cycle age model represents the most conservative option in terms of sedimentation rate and is in agreement with the initial age model of Westerhold and Röhl (2009) for the problematic interval but differs from it in the interpretation of the younger part of the records, where the initial age model significantly stretches the interval of Ec_{405} 13 and 14. We therefore choose our 2-cycle option as our preferred age model although more detailed stratigraphic work is needed. Further, the comparison with the GTS2012-based age model (Vandenberghe et al. 2012) adds to the uncertainties stemming from the discrepancy between radioisotopic and astronomical ages in this interval.

Finally, we established a fine tuning of the $\delta^{13}C$ records to the La2010d orbital solution, starting from our preferred 2-cycle age model. The good match between patterns observed in the proxy record and the orbital solution suggests that the newest astronomical solutions might be reliable back to 52 Ma, possibly until 54 Ma. Evidently, solving age model discrepancies for the early Eocene represents a critical step to understand the potentially complex response of the global carbon cycle during the early Eocene.

Acknowledgements. We are grateful to the International Ocean Discovery Program (IODP) for providing the samples used in this study. We thank two anonymous reviewers for their comments that significantly improved the manuscript. We thank A. van Dijk and D. Kasjanuk at Utrecht University for analytical support. This research was funded by NWO-ALW grant (project number 865.10.001) to L.J. Lourens.

References

Abels, H.A., Clyde, W.C., Gingerich, P.D., Hilgen, F.J., Fricke, H.C., Bowen, G.J., Lourens, L., 2012. Terrestrial carbon isotope excursions and biotic change during Palaeogene hyperthermals. Nature Geoscience **5**, 326–329, doi:10.1038/ngeo1427.

Agnini, C., Muttoni, G., Kent, D.V., Rio, D., 2006. Eocene biostratigraphy and magnetic stratigraphy from Possagno, Italy: The calcareous nannofossil response to climate variability. Earth and Planetary Science Letters **241**, 815–830, doi:10.1016/j.epsl.2005.11.005.

Agnini, C., Macri, P., Backman, J., Brinkhuis, H., Fornaciari, E., Giusberti, L., Luciani, V., Rio, D., Sluijs, A., Speranza, F., 2009. An early Eocene carbon cycle perturbation at ~52.5 Ma in the Southern Alps: Chronology and biotic response. Paleoceanography **24**, doi:10.1029/2008PA001649.

Aswasereelert, W., Meyers, S.R.R., Carroll, A.R.R., Peters, S.E.E., Smith, M.E.E., Feigl, K.L.L., 2012. Basin-scale cyclostratigraphy of the Green River Formation, Wyoming. Geological Society of America Bulletin **125**, 216–228, doi:10.1130/B30541.1.

Berggren, W.A., Pearson, P.N., 2005. A revised tropical to subtropical Paleogene planktonic foraminiferal zonation. The Journal of Foraminiferal Research **35**, 279–298. doi:10.2113/35.4.279

Berggren, W.A., Kent, D.V., Swisher III, C.C., Aubry, M.-P., 1995. A revised Cenozoic geochronology and chronostratigraphy. In: Berggren, W.A., Kent, D.V., Aubry, M.-P., Hardenbol, J. (Eds.), Geochronology, Time Scales and Global Stratigraphic Correlations: Framework for an Historical Geology, Special Publication SEPM, vol. **54**. SEPM (Society for Sedimentary Geology), Tulsa, OK, pp. 129–212.

Bouligand, C., Dyment, J., Gallet, Y., Hulot, G., 2006. Geomagnetic field variations between chrons 33r and 19r (83–41 Ma) from sea-surface magnetic anomaly profiles. Earth and Planetary Science Letters **250**, 541–560, doi:10.1016/j.epsl.2006.06.051.

Cande, S.C. and Kent, D.V., 1992. A New Geomagnetic Polarity Time Scale for the late Cretaceous and Cenozoic. Journal of Geophysical Research **97**, 13917–13951.

Cande, S.C., Kent, D.V., 1995. Revised calibration of the geomagnetic polarity timescale for the Late Cretaceous and Cenozoic. Journal of Geophysical Research **100**, 6093–6095.

Cramer, B.S., Wright, J.D., Kent, D.V., Aubry, M.-P., 2003. Orbital climate forcing of $\delta^{13}C$ excursions in the late Paleocene-early Eocene (chrons C24n–C25n). Paleoceanography **18**, doi:10.1029/2003PA000909.

Dickens, G.R., O'Neil, J.R., Rea, D.K., Owen, R.M., 1995. Dissociation of oceanic methane hydrate as a cause of the carbon isotope excursion at the end of the Paleocene. Paleoceanography **10**, 965–971, doi:10.1029/95PA02087.

Dickens, G.R., 2003. Rethinking the global carbon cycle with a large, dynamic and microbially mediated gas hydrate capacitor. Earth and Planetary Science Letters **213**, 169–183, doi:10.1016/S0012-821X(03)00325-X.

Galeotti, S., Krishnan, S., Pagani, M., Lanci, L., Gaudio, A., Zachos, J.C., Monechi, S., Morelli, G., Lourens, L., 2010. Orbital chronology of Early Eocene hyperthermals from the Contessa Road section, central Italy. Earth and Planetary Science Letters **290**, 192–200, doi:10.1016/j.epsl.2009.12.021.

Grant, K.M., Dickens, G.R., 2002. Coupled productivity and carbon isotope records in the southwest Pacific Ocean during the late Miocene-early Pliocene biogenic bloom. Palaeogeography, Palaeoclimatology, Palaeoecology, **187**(1–2), 61–82, doi:10.1016/S0031-0182(02)00508-4.

Kennett, J.P., Stott, L.D., 1991. Abrupt deep-sea warming, palaeoceanographic changes and benthic extinctions at the end of the Palaeocene. Nature **353**, 225–229, doi:10.1038/353225a0.

Kirtland Turner, S., Sexton, P.F., Charles, C.D., Norris, R.D., 2014. Persistence of carbon release events through the peak of early Eocene global warmth. Nature Geoscience **12**, 1–17, doi:10.1038/ngeo2240.

Komar, N., Zeebe, R.E., Dickens, G.R., 2013. Understanding long-term carbon cycle trends: The late Paleocene through the early Eocene. Paleoceanography **28**, 650–662, doi:10.1002/palo.20060.

Laskar, J., Robutel, P., Joutel, F., Gastineau, M., Correia, A.C.M., Levrard, B., 2004. A long-term numerical solution for the insolation. Astrononomy & Astrophysics, Volume **285**, 261–285.

Laskar, J., Fienga, A., Gastineau, M., Manche, H., 2011a. La2010: A new orbital solution for the long term motion of the Earth. Astronomy & Astrophysics, Volume **532**, A89.

Laskar, J., Gastineau, M., Delisle, J.-B., Farrés, A., Fienga, A., 2011b. Strong chaos induced by close encounters with Ceres and Vesta. Astronomy & Astrophysics **532**, L4, doi:10.1051/0004-6361/201117504.

Lauretano, V., Littler, K., Polling, M., Zachos, J.C., Lourens, L.J., 2015. Frequency, magnitude and character of hyperthermal events at the onset of the Early Eocene Climatic Optimum. Climate of the Past, accepted.

Littler, K., Röhl, U., Westerhold, T., Zachos, J.C., 2014. A high-resolution benthic stable-isotope record for the South Atlantic: Implications for orbital-scale changes in Late Paleocene-Early Eocene climate and carbon cycling. Earth and Planetary Science Letters **401**, 18–30, doi:10.1016/j.epsl.2014.05.054.

Lourens, L., Sluijs, A., Kroon, D., Zachos, J.C., Thomas, E., Röhl, U., Bowles, J., Raffi, I., 2005. Astronomical pacing of late Palaeocene to early Eocene global warming events. Nature **435**, 1083–1087, doi:10.1038/nature03814.

Ma, W., Tian, J., Li, Q., Wang, P., 2011. Simulation of long eccentricity (400-kyr) cycle in ocean carbon reservoir during Miocene Climate Optimum: Weathering and nutrient response to orbital change. Geophysical Research Letters, **38**, L10701, 10.1029/2011GL047680.

Machlus, M.L., Olsen, P.E., Christie-Blick, N., Hemming, S.R., 2008. Spectral analysis of the lower Eocene Wilkins Peak Member, Green River Formation, Wyoming: Support for Milankovitch cyclicity. Earth and Planetary Science Letters **268**, 64–75, doi:10.1016/j.epsl.2007.12.024.

Machlus, M.L., Ramezani, J., Bowring, S.A., Hemming, S.R., Tsukui, K., Clyde, W.C., 2015. A strategy for cross-calibrating U–Pb chronology and astrochronology of sedimentary sequences: An example from the Green River Formation, Wyoming, USA. Earth and Planetary Science Letters **413**, 70–78, doi:10.1016/j.epsl.2014.12.009.

Nicolo, M.J., Dickens, G.R., Hollis, C.J., Zachos, J.C., 2007. Multiple early Eocene hyperthermals: Their sedimentary expression on the New Zealand continental margin and in the deep sea. Geology **35**, 699, doi:10.1130/G23648A.1.

Paillard, D., Labeyrie, L., Yiou, P., 1996. Macintosh program performs time-series analysis. EOS AGU **77**, 379.

Reghellin, D., Coxall, H.K., Dickens, G.R., Backman, J., 2015. Carbon and oxygen isotopes of bulk carbonate in sediment deposited beneath the eastern equatorial Pacific over the last 8 million years. Paleoceanography, **30**, doi:10.1002/2015PA002825.

Sexton, P.F., Wilson, P.A., Pearson, P.N., 2006. Palaeoecology of late middle Eocene planktic foraminifera and evolutionary implications. Marine Micropaleontology **60**, 1–16, doi:10.1016/j.marmicro.2006.02.006.

Sexton, P.F., Norris, R.D., Wilson, P.A., Pälike, H., Westerhold, T., Röhl, U., Bolton, C.T., Gibbs, S.J., 2011. Eocene global warming events driven by ventilation of oceanic dissolved organic carbon. Nature **471**, 349–352, doi:10.1038/nature09826.

Slotnick, B.S., Dickens, G.R., Nicolo, M.J., Hollis, C.J., Crampton, J.S., Zachos, J.C., Sluijs, A., 2012. Large-amplitude variations in carbon cycling and terrestrial weathering during the latest Paleocene and earliest Eocene: The record at Mead Stream, New Zealand. The Journal of Geology **120**, 5, 487–505, doi:10.1086/666743.

Sluijs, A., Schouten, S., Donders, T.H., Schoon, P.L., Röhl, U., Reichart, G.J., Sangiorgi, F., Kim, J.-H., Sinninghe Damste, J.S., Brinkhuis, H., 2009. Warm and Wet Conditions in the Arctic Region during Eocene Thermal Maximum 2. Nature Geoscience **2**, 777–780.

Smith, M.E., Carroll, A.R., Singer, B.S., 2008. Synoptic reconstruction of a major ancient lake system: Eocene Green River Formation, western United States. Geological Society of America Bulletin **120**, 54–84, doi:10.1130/B26073.1.

Smith, M.E., Carroll, A.R., Scott, J.J., Singer, B.S., 2014. Early Eocene carbon isotope excursions and landscape destabilization at eccentricity minima: Green River Formation of Wyoming. Earth and Planetary Science Letters **403**, 393–406, doi:10.1016/j.epsl.2014.06.024.

Stap, L., Sluijs, A., Thomas, E., Lourens, L., 2009. Patterns and magnitude of deep sea carbonate dissolution during Eocene Thermal Maximum 2 and H2, Walvis Ridge, southeastern Atlantic Ocean. Paleoceanography **24**, doi: 10.1029/2008PA001655.

Stap, L., Lourens, L., Thomas, E., Sluijs, A., Bohaty, S., Zachos, J.C., 2010. High-resolution deep-sea carbon and oxygen isotope records of Eocene Thermal Maximum 2 and H2. Geology **38**, 607–610, doi:10.1130/G30777.1.

Suganuma, Y., Ogg, J.G., 2006. Campanian through Eocene magnetostratigraphy of Sites 1257–1261, ODP leg 207, Demerara Rise (western equatorial Atlantic). Proceedings of the Ocean Drilling Program, Scientific Results, Volume **207**.

Tsukui, K., Clyde, W.C., 2012. Fine-tuning the calibration of the early to middle Eocene geomagnetic polarity time scale: Paleomagnetism of radioisotopically dated tuffs from Laramide foreland basins. Geological Society of America Bulletin **124**, 870–885, doi:10.1130/B30545.1.

Vandenberghe, N., Hilgen, F.J., Speijer, R.P., 2012. The Paleogene Period. In: Gradstein, F., Ogg, J., Schmitz, M., Ogg, G. (eds.), The Geological Time Scale 2012. Elsevier, Amsterdam, 855–921.

Wade, B.S., Pearson, P.N., Berggren, W.A., Pälike, H., 2011. Review and revision of Cenozoic tropical planktonic foraminiferal biostratigraphy and calibration to the geomagnetic polarity and astronomical time scale. Earth-Science Reviews **104**, 111–142. doi:10.1016/j.earscirev.2010.09.003

Westerhold, T., Röhl, U., Laskar, J., Raffi, I., Bowles, J., Lourens, L., Zachos, J.C., 2007. On the duration of magnetochrons C24r and C25n and the timing of early Eocene global warming events: Implications from the Ocean Drilling Program Leg 208 Walvis Ridge depth transect. Paleoceanography **22**, doi:10.1029/2006PA001322.

Westerhold, T., Röhl, U., Raffi, I., Fornaciari, E., Monechi, S., Reale, V., Bowles, J., Evans, H.F., 2008. Astronomical calibration of the Paleocene time. Palaeogeography, Palaeoclimatology, Palaeoecology **257**, 377–403, doi:10.1016/j.palaeo.2007.09.016.

Westerhold, T., Röhl, U., 2009. High resolution cyclostratigraphy of the early Eocene – new insights into the origin of the Cenozoic cooling trend. Climate of the Past **5**, 309–327, doi: 10.5194/cp-5-309-2009.

Westerhold, T., Röhl, U., Laskar, J., 2012. Time scale controversy: Accurate orbital calibration of the early Paleogene. Geochemistry, Geophysics, Geosystems **13**, Q06015, doi: 10.1029/2012GC004096.

Westerhold, T., Röhl, U, Frederichs, T., Bohaty, S.M., Zachos, J.C., 2015 Astronomical calibration of the geological timescale: closing the middle Eocene gap. Climate of the Past **11**, 1181–1195, doi:10.5194/cp-11-1181-2015.

Zachos, J.C., Pagani, M., Sloan, L., Thomas, E., Billups, K., 2001. Trends, rhythms, and aberrations in global climate 65 Ma to present. Science **292**, 686–693.

Zachos, J.C., Kroon, D., Blum, P. et al., 2004. ODP Leg 208: The early Cenozoic extreme climates transect along walvis ridge, Proceedings of the Ocean Drilling Program, Initial Reports, **208**.

Zachos, J.C., Röhl, U., Schellenberg, S.A., Sluijs, A., Hodell, D.A., Kelly, D.C., Thomas, E., Nicolo, M., Raffi, I., Lourens, L.J., McCarren, H., Kroon, D., 2005. Rapid acidification of the ocean during the Paleocene–Eocene thermal maximum. Science **308**, 1611–1615, doi:10.1126/science.1109004.

Zachos, J.C., Dickens, G.R., Zeebe, R.E., 2008. An early Cenozoic perspective on greenhouse warming and carbon-cycle dynamics. Nature **451**, 279–283, doi:10.1038/nature06588.

Zachos, J.C., McCarren, H., Murphy, B., Röhl, U., Westerhold, T., 2010. Tempo and scale of late Paleocene and early Eocene carbon isotope cycles: Implications for the origin of hyperthermals. Earth and Planetary Science Letters **299**, 242–249, doi:10.1016/j.epsl.2010.09.004.

Manuscript received: September 9, 2015; rev. version accepted: January 7, 2016.

The following appendices are available under http://doi.pangaea.de/10.1594/PANGAEA.857763

Appendix A: Benthic stable isotope data of ODP Site 1263.
Appendix B: Supplementary information.